


Conjoint influence of quantum interference and Freeman resonance on substructures of the photoelectron spectra in above-threshold ionization

Shun Wang, Wei-Chao Jiang ,* Xiao-Qing Tian, and Hui-Bin Sun

College of Physics and Optoelectronic Engineering, Shenzhen University, Shenzhen 518060, China



(Received 16 December 2019; revised manuscript received 30 March 2020; accepted 21 April 2020; published 8 May 2020)

Based on the numerical solution of the full-dimensional time-dependent Schrödinger equation, we study the above-threshold ionization of atomic hydrogen by subpicosecond laser pulses at wavelengths ranging from 300 nm to 800 nm, in which regime substructures of the photoelectron energy spectra resulting from quantum interference are entangled with those induced by the Freeman resonance. By analyzing the time-dependent populations and ac Stark energy shifts of the relevant atomic levels, and observing the pulse intensity dependence and the pulse length evolution of the spectra, we clearly identify the origins of the substructures exhibited in the spectra.

DOI: [10.1103/PhysRevA.101.053417](https://doi.org/10.1103/PhysRevA.101.053417)

I. INTRODUCTION

Above-threshold ionization (ATI) refers to the intense-laser-pulse-stimulated photoionization process during which the number of photons absorbed by the bound electron exceeds the minimum number necessary for the electron to be emitted. This phenomenon was first experimentally observed as early as 40 years ago [1], when the photoelectron energy spectrum for the ionization of xenon atoms was found to have a double-peak structure, indicating an additional photon absorption. Ever since then, ATI, a type of nonperturbative effect, has been observed in a variety of atoms and molecules [2–8], and its study has all along been one of the most important topics in strong-field physics. Among various aspects of ATI, fine structures of ATI peaks, from which important information of the related physical processes can be extracted, are a subject of particular interest. For example, under certain conditions, one ATI primary peak is observed to break up into a series of narrow subpeaks. This phenomenon of peak splitting may originate from different mechanisms. Two typical mechanisms of the peak splitting are quantum interference [9,10] and the Freeman resonance [11–17], either of which has been intensively studied for years, both theoretically and experimentally.

Quantum interference can originate from the ac-Stark-shift-induced ionization bursts at different times. At the two symmetrical time points, located on the rising and falling edges of the laser pulse, respectively, two electron wave packets are produced from the equally ac-Stark-shifted atomic level. The interference between the two temporally separated electron wave packets can lead to the peak splitting in the photoelectron energy spectrum. The modulation of the photoelectron spectrum by quantum interference has been extensively discussed by different authors [9,10,18–21]. In

particular, quantum interference in the case where the energy of one photon is large enough to ionize the bound electron, often termed “dynamic interference”, has attracted a lot of attention in recent years [18–20,22,23].

Freeman-resonance-induced fine structure is also related to the ac Stark shifts of atomic levels [11,24]. As the laser pulse rises and falls, the ac Stark effect successively sweeps a series of Rydberg states into and out of resonance. The electron population is thus efficiently transferred to the Rydberg states from the ground state, and the ionization via the Rydberg states is considerably enhanced. Electrons emitted from different Rydberg states via absorption of the same number of photons will have different final kinetic energies, leading to subpeaks in the ATI spectrum. Freeman resonance has proven to be a universal phenomenon. Since its discovery, it has been found not only in a lot of atoms [11–17,25,26], but also in a number of molecules [27–30]. Accompanying these experimental discoveries, numerous analytical [31–34] and numerical [9,35–38] calculations also have been carried out to analyze the underlying physics. However, due to the large box required to describe the wave functions of the high-lying Rydberg states, and also due to the rather long pulse length (subpicosecond) necessary for distinguishing the small energy gaps between the high-lying Rydberg states, precisely studying the dynamics of the Freeman resonance by numerically solving the full-dimensional time-dependent Schrödinger equation (TDSE) is not an easy task. Even a full-dimensional TDSE calculation that produces distinct Freeman resonance subpeaks is rarely seen today [39,40]. Some TDSE studies [10,37] involving the Freeman resonance only dealt with laser pulses up to 20 fs, for which the energy gaps between the Rydberg states cannot be recognized. Therefore, the authors only observed broadenings of the main ATI peaks, but not the emergence of resonance-induced subpeaks. Besides the Freeman-resonance-induced peak splitting, another strong field phenomena, known as resonancelike enhancement [41,42], also has been deemed attributable to resonances of the

*jiang.wei.chao@szu.edu.cn

excited states by many [43–46]. However, its physical origin is still under controversy [47].

Given the two different mechanisms responsible for the peak splitting in the photoelectron spectrum, the question arises naturally as to whether these two mechanisms can coexist in the ionization process and how they combinedly influence the photoelectron spectrum. By solving the TDSE for a one-dimensional model hydrogen atom in the Kramers-Henneberger frame, Reed *et al.* [9] found that both quantum interference and Freeman resonance contribute to the detailed structure of the ATI spectrum. Depending on parameters of the laser pulse, both of the two mechanisms may play a role, or only one of them plays a noticeable role. Blank *et al.* [48] studied the effects of quantum interference between resonantly enhanced ionization pathways. The purpose of this paper is to present a full-dimensional TDSE study of the roles played by quantum interference and the Freeman resonance conjointly in the ionization of atomic hydrogen by subpicosecond laser pulses, with an emphasis on their influence on substructures of the photoelectron energy spectrum.

The rest of this paper is structured as follows. In the next section, we briefly review the TDSE numerical method, describe the laser parameters used in the calculations, and introduce the scheme for calculating the ac Stark shift. In Sec. III, we present our numerical results and interpret the phenomena observed in the electron spectra. In the last section, we summarize the main results and findings of this paper.

II. THEORY AND METHOD

A. TDSE calculation

The time evolution of the single-electron wave function $\Psi(\mathbf{r}, t)$ is described by the following TDSE (atomic units are used throughout the paper unless explicitly stated):

$$i \frac{\partial}{\partial t} \Psi(\mathbf{r}, t) = H \Psi(\mathbf{r}, t), \quad (1)$$

where the Hamiltonian is composed of the electron kinetic energy T , the Coulomb potential V , and the laser-electron coupling $H_1(t)$. In this work, we use the velocity gauge, in which the laser-electron coupling is written as

$$H_1(t) = -i\mathbf{A}(t) \cdot \nabla, \quad (2)$$

with $\mathbf{A}(t)$ being the vector potential of the pulse. For atomic hydrogen, the Coulomb potential V is explicitly given by $V = -1/r$. To solve the TDSE, we adopt the recently proposed numerical method which uses the split-Lanczos propagator to propagate the wave function in time [49]. By splitting out the centrifugal potential from the Hamiltonian, the efficiency of the traditional Lanczos propagator is greatly improved. The splitting error is controlled by the preset time step Δt . To reduce the propagation error, the algorithm introduces a mechanism that dynamically determines the optimal time step for each propagation based on Δt . In our calculations, the wave function is expressed uniquely as a sum of spherical harmonic functions, and the radial part of the wave function is discretized using the finite-element discrete variable representation (FE-DVR) method [50–52]. To avoid the use of very large radial box, the wave-splitting technique [53] is adopted.

Linearly polarized laser pulse with a carrier wavelength λ of 300–800 nm and a peak intensity I of the order of 10^{14} W/cm² is used. Because of the linear polarization, the atomic system possesses the cylindrical symmetry, and the magnetic quantum number is conserved. The vector potential $\mathbf{A}(t)$ is chosen to be

$$\mathbf{A}(t) = \mathbf{A}_0 g(t) \sin \omega t, \quad (3)$$

where ω is the carrier angular frequency, \mathbf{A}_0 a constant vector potential, and $g(t)$ the envelope function. In most of our calculations, we adopt the sine-squared pulse whose envelope function is

$$g(t) = \sin^2 \frac{\pi(t + T/2)}{T}, \quad -T/2 < t < T/2 \quad (4)$$

and $g(t) = 0$ elsewhere. For this type of pulse, the full width at half maximum (FWHM) is half of the pulse duration T . Considering the fact that the sine-squared pulse has a quite artificial envelope and is experimentally unrealistic, in Sec. III E, a comparison is made between the electron spectra produced by the sine-squared pulse and a pulse closer to those used in strong field experiments, the Gaussian pulse, whose envelope is described by

$$g(t) = \exp \left[-\ln(2) \left(\frac{2t}{\tau} \right)^2 \right] \quad (5)$$

for the time interval $(-2\tau, 2\tau)$ and $g(t) = 0$ elsewhere (τ represents the FWHM).

In our calculations, FWHM = 0.1 – 0.4 ps is chosen. To ensure the numerical convergence, for a given laser pulse, we perform a series of calculations with increasing radial box size R and number of angular momenta kept n_L , and decreasing preset time step Δt . When the obtained electron energy spectrum stops varying with changes of these parameters, numerical convergence is achieved. After a careful check, we find that $n_L = 15$, $R = 2000$ a.u., and $\Delta t = 0.01$ a.u. is sufficient to ensure the convergence for laser parameters chosen in this work. To take account of the high-lying excited states whose wave functions are more spatially extensive, large radial box is inevitable, even when the wave-splitting technique [53] or the time-dependent surface flux technique [54–56] (which has been designed for decreasing the box size needed) is employed.

From here onwards, if not otherwise indicated, the sine-squared pulse is used.

B. Calculation of the ac Stark energy shift

The probability amplitude $a_E(t)$ for populating the continuum state with energy E , which can be exactly derived from the TDSE, reads [22]

$$a_E(t) = -i e^{-iEt} \sum_j \mathbf{p}_{Ej} \cdot \int_{-\infty}^t \mathbf{A}(\tau) a_j(\tau) e^{iE\tau} d\tau, \quad (6)$$

where $a_j(t) = \langle \Psi_j | \Psi(t) \rangle$ is the time-dependent projection amplitude of the wave function at t , $|\Psi(t)\rangle$, to the eigenstate of the field-free Hamiltonian, $|\Psi_j\rangle$. $\mathbf{p}_{Ej} = \langle \Psi_E | -i\nabla | \Psi_j \rangle$ is the transition matrix element. If the transition from a bound state $|\Psi_j\rangle$ to the final continuum state plays a dominant role

over transitions through all other channels, Eq. (6) is reduced to

$$a_E^j(t) = -i e^{-iEt} \mathbf{p}_{Ej} \cdot \int_{-\infty}^t \mathbf{A}(\tau) a_j(\tau) e^{iE\tau} d\tau. \quad (7)$$

In our previous work on dynamic interference [22], Eq. (7) was used to analyze the interference patterns in the case where the transition from the ground state is dominant. In the present work, Eq. (7) can be used to predict the energy positions of subpeaks induced by Freeman resonances of particular intermediate excited states.

In our numerical calculations, the ac Stark shift of a bound state is obtained as follows. The initial state, from which the TDSE wave function evolves in time, is chosen to be the state whose ac Stark shift is to be calculated. The projection amplitude $a_j(t)$ obtained can be written as

$$a_j(t) = f(t) e^{-i\phi(t)}, \quad (8)$$

where $f(t)$ and $\phi(t)$ are $a_j(t)$'s modulus and phase, respectively. When the external laser field is off, Eq. (8) is reduced to $a_j(t) = \exp(-iE_j t)$, i.e., $f(t) = 1$ and $\phi(t) = E_j t$, with E_j being the eigenenergy of $|\Psi_j\rangle$. The time derivative of $\phi(t)$, $\frac{d\phi(t)}{dt}$, equals the energy E_j . In the presence of laser field, $\frac{d\phi(t)}{dt}$ is assumed to be the instantaneous energy of level j ; since the laser field is rapidly oscillating, the $\frac{d\phi}{dt}$ - t curve is also rapidly oscillating. One may smooth the curve by means of the mean filtering or the Fourier filtering technique, to filter out the unimportant, high-frequency components and effectively obtain a cycle-averaged quantity, that is, the time-dependent ac-Stark-shifted energy $E_j(t)$. This scheme for calculating the ac Stark shift was applied with considerable success to the determination of the ac Stark shift of the ground state in our previous work [22]. However, this scheme relies heavily on the electron population. $\frac{d\phi(t)}{dt}$ produces correct instantaneous energy only when the population is large enough, whereas, for small population, $\frac{d\phi(t)}{dt}$ gives unreasonable result. Segments that are unreasonable in the $\frac{d\phi}{dt}$ - t curve should be deleted first, before the smoothing treatment of the curve.

As a test of the above-described scheme, we calculate the ac-Stark-shifted ground-state energy of atomic hydrogen subjected to a 400 nm laser pulse with peak intensity of 1.7×10^{14} W/cm² and FWHM of 0.4 ps. The result is plotted in Fig. 1 (dashed line), which has been smoothed using mean filtering. A small segment lying slightly before $t = 5000$ a.u. in the curve has been deleted, for the unreasonable values of the ac-Stark-shifted energy obtained in this segment.

The ac-Stark shifts or the quasienergies of atomic levels are gauge dependent [20,36,57]. If one includes the \mathbf{A}^2 term in the velocity gauge, i.e., $H_I(t) = -i\mathbf{A} \cdot \nabla + \mathbf{A}^2/2$, the energy shifts of levels are the same as those in the length gauge [$H_I(t) = \mathbf{F} \cdot \mathbf{r}$ with \mathbf{F} being the electric field]. But the ac Stark shift ΔE^V in the velocity gauge excluding the \mathbf{A}^2 term [Eq. (2)] is different from the shift ΔE^L in the length gauge, and $\Delta E^V = \Delta E^L - U_p$ with U_p being the ponderomotive energy. While the ac Stark shifts of atomic levels are gauge dependent, the time-varying energy separations between levels are not. Therefore, different gauges of the electron-laser interaction describe the same physics. In length-gauge description of photoemission when the photon energy is much

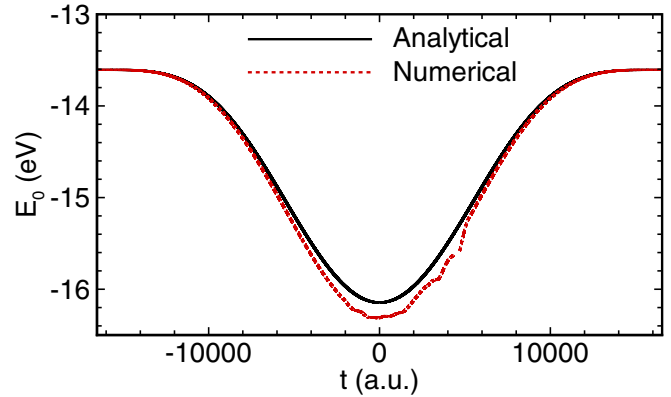


FIG. 1. Ground-state energy as a function of time obtained numerically (dashed line) and analytically [Eq. (10)] (solid line) for a 400 nm laser pulse with $I = 1.7 \times 10^{14}$ W/cm² and FWHM = 0.4 ps. The dashed line has been smoothed using mean filtering.

smaller than the ionization potential of atoms, the ground state is negligibly shifted, whereas the high-lying Rydberg states coshift with the continuum, approximately by U_p . Similar description of the ac Stark shifts of the ground state and the continuum frequently appears in the context of ATI without explicitly stressing the gauge involved [13,15,16,31]. In the present velocity gauge [Eq. (2)], the above description should be changed: now the energy shifts of both high-lying Rydberg states and the continuum are negligible, while the ac Stark shift of the ground state can be estimated using the analytical expression of the ponderomotive energy, i.e.,

$$\Delta E_0(t) = -U_p(t) = -\frac{[F_0(t)]^2}{4\omega^2}, \quad (9)$$

where $F_0(t)$ is the instantaneous amplitude of the electric field, which evolves with time following the pulse envelope. The time-dependent ground-state energy is thus written as

$$E_0(t) = E_0 + \Delta E_0(t), \quad (10)$$

where E_0 (≈ 13.6 eV) is the field-free ground-state energy. This function is plotted in Fig. 1 (solid line) for comparison with the numerical result (dashed line) from TDSE. The two curves almost coincide with each other for $t < -9000$ a.u. and $t > 9000$ a.u. For other range of t , the two curves can still be considered consistent with each other, although a small discrepancy appears between them. Comparison between the two curves implies that the assumption that the ac Stark shift of the ground state equals $-U_p(t)$ [Eq. (9)] is more valid at lower laser intensities.

III. RESULTS AND DISCUSSIONS

A. Global structure of the photoelectron energy spectrum

Figure 2 shows the photoelectron energy spectrum for ionization of the ground-state atomic hydrogen by a subpicosecond laser pulse with peak intensity $I = 1.7 \times 10^{14}$ W/cm², wavelength $\lambda = 400$ nm, and FWHM = 0.4 ps. The whole spectrum consists of a series of ATI orders which are separated from each other by the energy of one photon (approximately 3.1 eV), characterizing the typical construction of

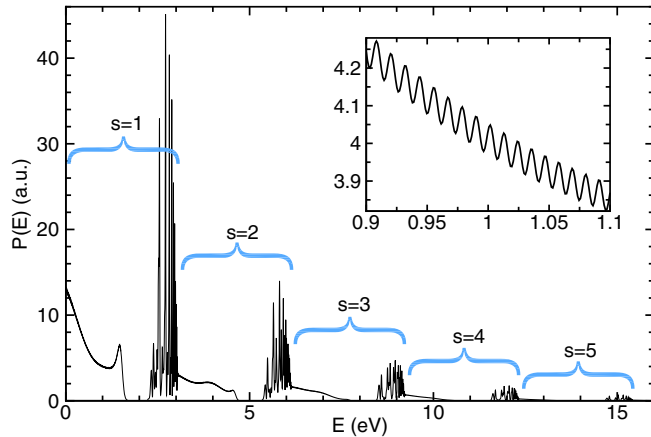


FIG. 2. Spectrum (in linear scale) of photoelectrons emitted from the ground-state H atom subjected to a 400 nm laser pulse with $I = 1.7 \times 10^{14} \text{ W/cm}^2$ and FWHM = 0.4 ps. Inset: expanded spectrum in the range of 0.9–1.1 eV.

an ATI spectrum. Only the first five ATI orders are shown, since higher ATI orders are not as visible. The structure of the ATI orders is quite distinctive: each ATI order is composed of two distinct parts—a smooth tail-like segment and a spiky main ATI peak. Each tail-like segment has a fine structure—in closeup view the curve appears to oscillate rapidly. For example, the inset of Fig. 2 shows the expanded spectrum in the range of 0.9–1.1 eV (part of the first tail), in which a fast oscillation of the curve is clearly seen. In the first tail-like segment, the envelope of the spectrum shows a prominent single peak in its right part. This single peak of the spectrum envelope becomes much more indistinct in the second tail-like segment and completely disappears in other tails. Each main ATI peak also exhibits a substructure, composed of a series of narrow subpeaks, as can be seen in the figure.

The structure of the spectrum reflects information of the ionization process. The electron may first jump to an excited state by absorbing some number of photons and then absorb s additional photons to escape the atom. The electron also might be directly emitted from the ground state by absorbing s photons. In the spectrum shown in Fig. 2, a given s is associated with a particular ATI order, as denoted by the blue braces. The tail-like structures and the main ATI peaks correspond to electrons emitted from the low-lying bound states and the high-lying ones, respectively. The height of the main ATI peak, as well as the signal of the tail-like structure, decreases significantly with an increase in s .

B. Oscillations in the tail-like structures

Observing the tail-like structures shown in Fig. 2 in closeup, we find that each tail contains a substructure characterized by a fast oscillation (see, e.g., the inset of Fig. 2). Generally speaking, energy positions and heights of subpeaks arising from quantum interference are highly sensitive to variations of the pulse intensity and length. In contrast, positions of subpeaks due to the Freeman resonance are roughly constant against the change in pulse intensity or duration, because they are associated with intermediate excited states whose energy shifts relative to the continuum are tiny. To

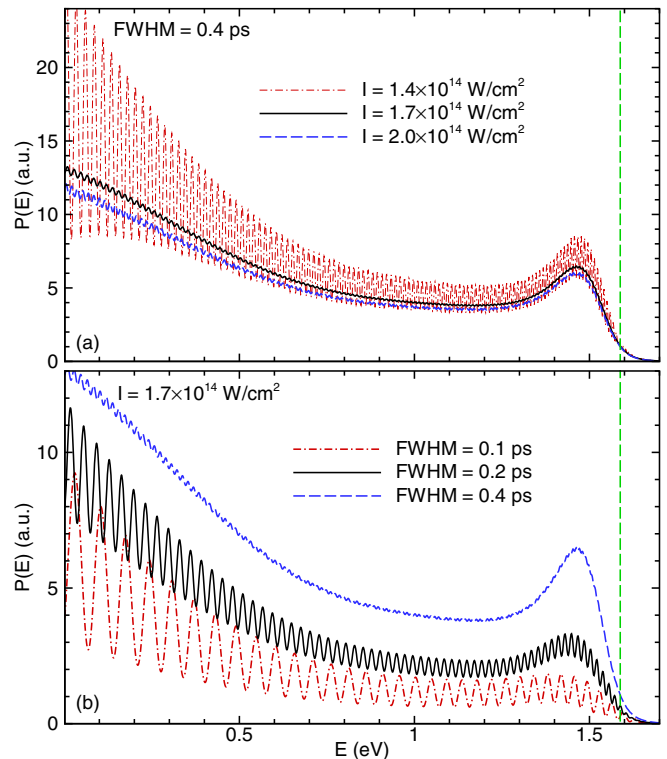


FIG. 3. Dependence of the first tail-like structure (in linear scale) on peak intensity (a) and FWHM (b) of the laser pulse. The vertical dashed lines mark the energy position of the Freeman resonance peak related to levels with $n = 3$ predicted without considering the ac Stark shift.

identify the natures of the subpeaks in the tail-like structures, we show the first tail-like structures of the spectra for pulses of varying intensities and pulses of varying lengths in Figs. 3(a) and 3(b), respectively. In Fig. 3(a), all three curves show an oscillating behavior. The amplitude of the oscillation is significant when the laser intensity is low ($I = 1.4 \times 10^{14} \text{ W/cm}^2$), and decreases rapidly as the intensity is increased. The energy positions of the small peaks and the spacing between them also change with varying laser intensity. In Fig. 3(b), the oscillating amplitude of the curve decreases quickly with the increase in pulse length. Moreover, the spacing between the small subpeaks shows a fast decrease with increasing pulse length as well. The dependence of the tail-like structure on pulse intensity and duration shown in Figs. 3(a) and 3(b) clearly indicates that the observed oscillatory behavior is attributable to quantum interference.

Besides the large number of small peaks observed in each tail-like structure, the envelope of the spectrum also exhibits a single peak, which is much broader, at around 1.46 eV. This single peak is insusceptible to pulse intensity or duration, which is a clear signature of the Freeman resonance. Without taking account of the tiny ac Stark shift of the intermediate excited state, the energy position of a Freeman resonance subpeak is given by

$$E = s\omega + E_0/n^2, \quad (11)$$

where n is the principal quantum number of the intermediate state. Only the energy position with $n = 3$ predicted by

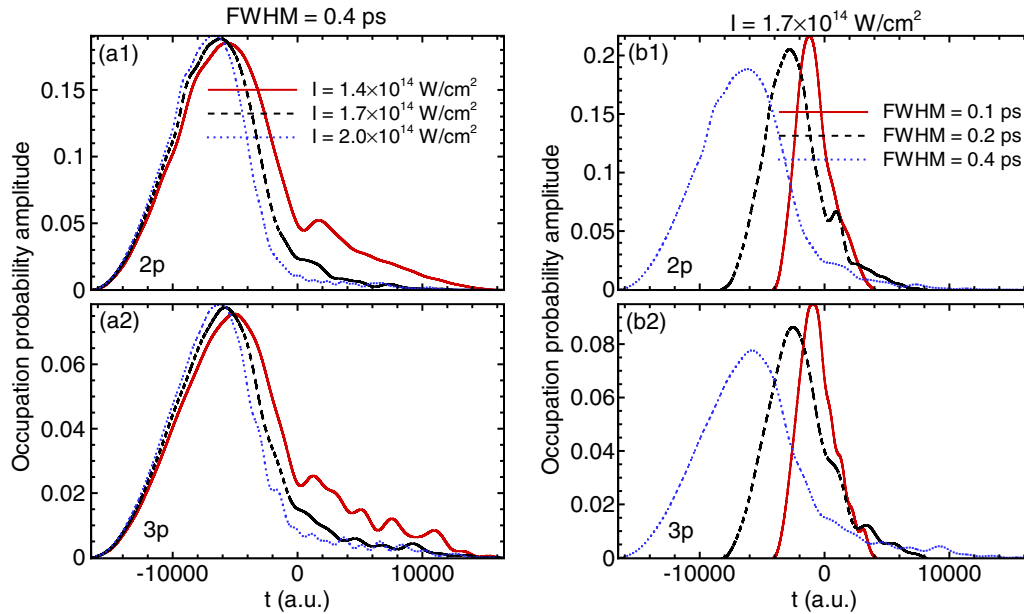


FIG. 4. Occupation probability amplitudes of the $2p$ and $3p$ states as functions of time for pulses of varying peak intensities (a1), (a2) and pulses of varying durations (b1), (b2). The origin of time axis is set to coincide with the center of the laser pulse. All curves have been smoothed via Fourier filtering.

Eq. (11) lies in the energy range covered in Fig. 3, as marked by the vertical dashed lines. The single peak of the spectrum envelope is therefore identified as due to Freeman resonances of levels with $n = 3$, intermediated by four photons. The discrepancy between the position of the single peak and that of the vertical dashed line can be interpreted in terms of the ac Stark energy shifts of the $n = 3$ levels. In addition to the ejection of electrons from levels with $n = 3$ via one-photon absorption, the ionization directly from the ac-Stark shifted ground state via five-photon absorption can also contribute to the single peak near 1.46 eV.

The dependence of the interference pattern in the tail-like structure on laser intensity and duration can be well understood in a simple time-domain double-slit interference scenario. In such a scenario, the double slits are opened up at two instantaneous times, which are respectively on the rising and falling edges of the laser pulse. Numerous pairs of such double slits are opened up during the process of the laser-atom interaction, and each pair corresponds to a particular kinetic energy of the ionized electron. One necessary condition for the double slits to open up and thus for the interference to occur is that the ionization is not completed before the pulse peak arrives [20]. A more intense or longer laser pulse results in a larger electron depletion and thus a smaller electron population in the second half of the pulse, as can be seen from Fig. 4, where, as examples, the (smoothed) occupation probability amplitudes of the $2p$ and $3p$ states as functions of time for pulses of varying peak intensities [Figs. 4(a1) and 4(a2)] and pulses of varying durations [Figs. 4(b1) and 4(b2)] are plotted. It is this decrease in the population at the second one of the two slits that leads to the interference pattern diminishing. In addition, as seen in Figs. 4(b1) and 4(b2), a longer pulse enables the opening up of more pairs of double slits in a wider time range. Therefore, for a longer pulse, the phase difference between electron wave packets ejected at

the double slits varies faster with the energy of the ionized electron, leading to the narrower spacing between subpeaks in the spectrum.

C. Substructures in the main ATI peaks

To examine in more detail the substructures of the main ATI peaks, we present a closeup depiction of the first three main ATI peaks in the photoelectron spectra for pulses of varying intensities but identical durations in Fig. 5, where, for each intensity, the three main peaks are plotted respectively from top to down. A large amount of subpeaks can be clearly seen. Evidently, subpeaks whose energy positions are insensitive to laser intensity changes arise as a result of the Freeman resonance. The vertical dashed lines mark subpeak positions predicted in the spirit of the Freeman resonance without taking account of the energy shifts of the intermediate excited states, i.e., from Eq. (11). The conspicuous discrepancies between subpeak positions predicted via Eq. (11) and those observed from the spectra indicate that, to interpret the fine structures of the main ATI peaks, the tiny ac Stark shifts of the intermediate sublevels with respect to the ionization threshold cannot be overlooked. The subpeak corresponding to $I = 1.7 \times 10^{14} \text{ W/cm}^2$ near 2.55 eV deviates from the predicted position by $7.8 \times 10^{-3} \text{ eV}$. With increasing n , the predicted positions and the observed ones agree with each other better. This is because the energy shift of a sublevel decreases with an increase in n . Moreover, it can be seen that the subpeak positions slightly change when the laser intensity is changed (for example, the subpeak near 2.55 eV shifts leftwards by $3.5 \times 10^{-3} \text{ eV}$ as I is increased from $1.7 \times 10^{14} \text{ W/cm}^2$ to $2.0 \times 10^{14} \text{ W/cm}^2$), which is in consistency with the fact that the ac Stark shift is dependent on laser intensity.

To identify which intermediate sublevels are relevant to the observed subpeaks in the spectra, in Figs. 6(a) and 6(b), for

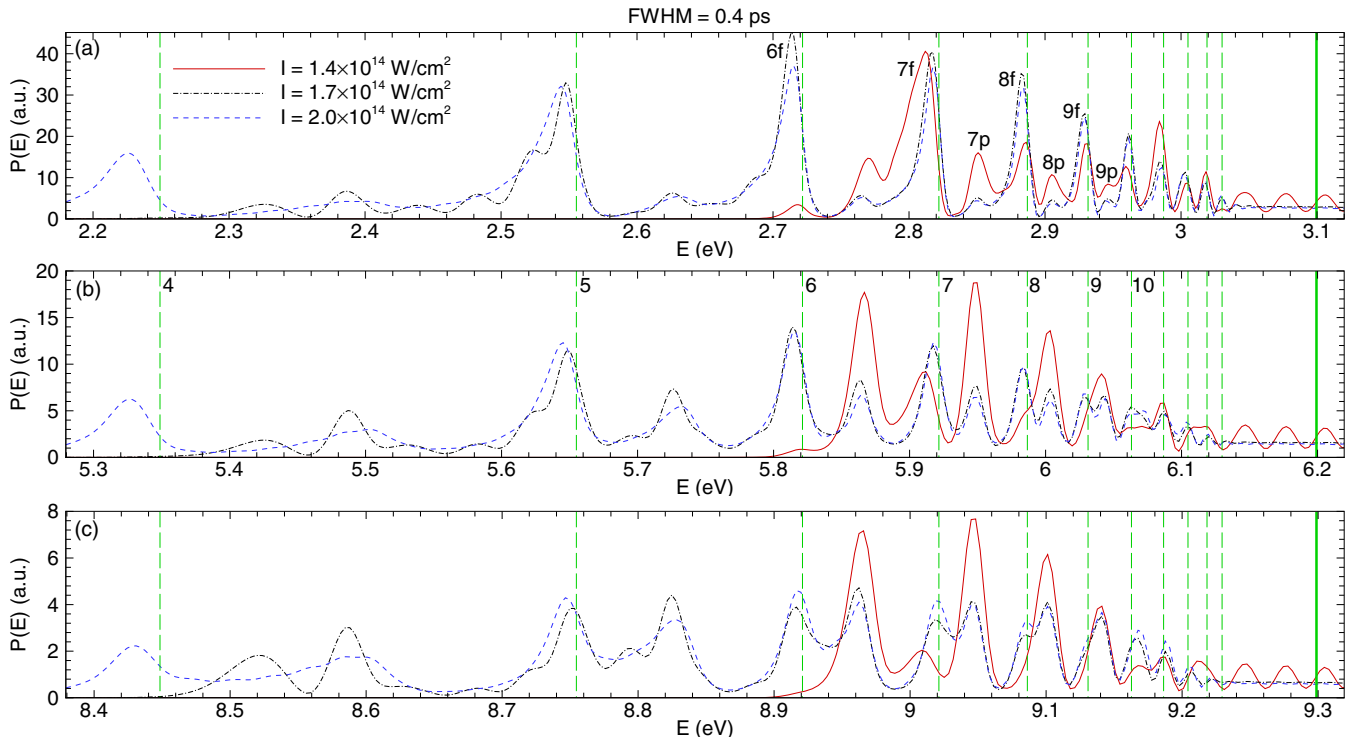


FIG. 5. Detailed structures of the first three main ATI peaks [plotted (in linear scale) in (a)–(c), respectively] in the spectra for pulses of varying peak intensities but identical FWHM. The vertical dashed lines mark subpeak positions predicted in the spirit of the Freeman resonance without considering the ac Stark shifts of the intermediate states. Integers next to the lines [shown in (b) only] are quantum numbers n of the intermediate states. The thicker vertical solid lines mark the predicted subpeak positions in the $n \rightarrow \infty$ limit. The nl numbers denote the identified sublevels related to the subpeaks.

laser intensity $I = 1.7 \times 10^{14} \text{ W/cm}^2$, we show respectively the dependence of the time-averaged electron population and the population at the end of the pulse on the angular momentum quantum number l for $n = 3 - 12$. For $n \geq 6$, the time-averaged electron population at $l = 1$ and $l = 3$ is at least one order of magnitude larger than at any other value of l . Since large population is gained via the resonance-induced population transfer, we infer that the p and f sublevels are those ac Stark shifted into resonance and thus a major contribution to the substructures of the main ATI peaks. We further infer that these two sublevels are still dominant in the case of other laser parameters used in this subsection.

In the following, we will only be concerned with these two sublevels when calculating the ac Stark shift. As to the final electron populations [Fig. 6(b)], populations of sublevels with odd (even) l exhibit a dominance over those with even (odd) l , for $n > 3$ ($n = 3$). This is a clear indication that Freeman resonances via the absorption of an odd (even) number of photons are more prevalent for levels with $n > 3$ ($n = 3$), because the absorption of one photon varies l by only one unit. Indeed, the population transfer to the $n = 3$ states is identified as through a four-photon resonance, whereas population transfers to the $n > 3$ states are due to five-photon resonances. For laser intensity $I = 1.7 \times 10^{14} \text{ W/cm}^2$, we have calculated the

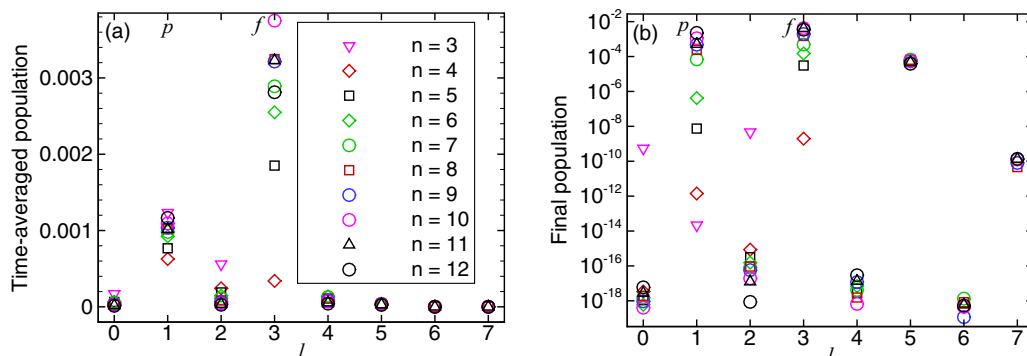


FIG. 6. Time-averaged electron population (a) and the final electron population (b) as functions of the quantum number l for different n in the case of $I = 1.7 \times 10^{14} \text{ W/cm}^2$ and FWHM = 0.4 ps.

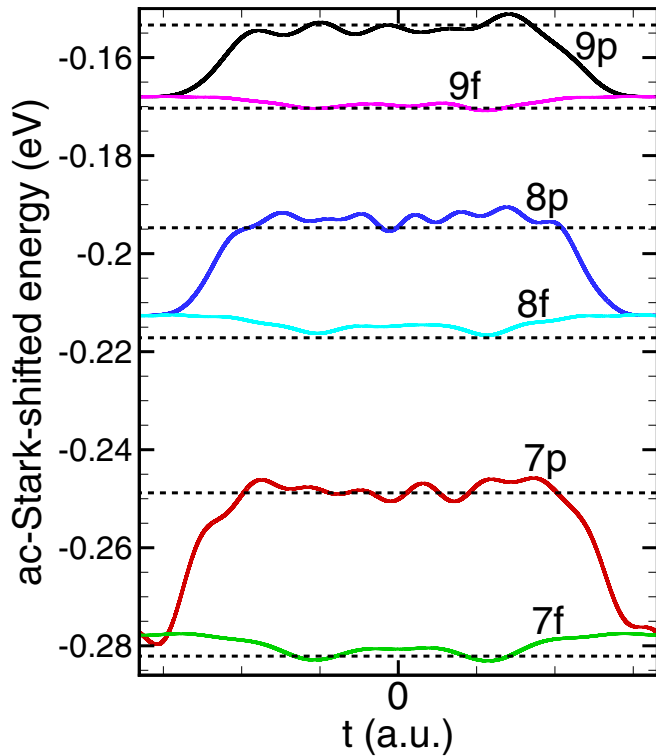


FIG. 7. Time-varying ac-Stark-shifted energies of the high-lying excited states with $n = 7, 8, 9$ and $l = 1, 3$ in the case of $I = 1.7 \times 10^{14} \text{ W/cm}^2$ and FWHM = 0.4 ps. Horizontal dashed lines denote energies obtained by subtracting the photon energy from the energies at which the spectrum for $I = 1.7 \times 10^{14} \text{ W/cm}^2$ peaks in the range of 2.8–2.95 eV in Fig. 5(a).

ac-Stark-shifted energies of the np and nf states with $n = 7, 8,$ and 9 as functions of time using the method described in Sec. II. The results are plotted in Fig. 7. It can be seen that the energy shifts of these high-lying excited states are quite tiny, in comparison with that of the ground state (Fig. 1). On this point, our calculation agrees well with previous studies [36,58]. Furthermore, the np sublevels shift upwards in energy, whereas the nf sublevels shift downwards but with much smaller magnitude. Once the ac Stark energy shifts are obtained, the link between the resonance-induced subpeaks and the intermediate sublevels can be easily established. For example, for all subpeaks located in the range of 2.8–2.95 eV in the spectrum corresponding to $I = 1.7 \times 10^{14} \text{ W/cm}^2$ in Fig. 5(a), the energies of the relevant sublevels at the time of ionization can be approximated by $E - \omega$, with E being the subpeak energy positions. Then, in Fig. 7, we draw horizontal lines whose vertical coordinates are $E - \omega$. A simple comparison between the horizontal lines and the curves for the time-varying ac-Stark-shifted energies enables a clear identification of sublevels relevant to the subpeaks. The identified sublevels are indicated next to the corresponding subpeaks in Fig. 5(a) using the nl quantum numbers. Although the identification is done for the spectrum for $I = 1.7 \times 10^{14} \text{ W/cm}^2$, the nl notations are also applicable to subpeaks in the spectra for the other two intensities. In the same approach, we also identify the subpeaks near 2.72 eV in Fig. 5(a) as being due to the 6f Freeman resonance.

The spectra between the vertical dashed lines of $n = 4$ and $n = 5$ in Figs. 5(a)–5(c) are more complicated. While the subpeaks near the vertical lines of $n = 5$ are Freeman resonance peaks related to the $n = 5$ levels, it is not easy to allocate other subpeaks to specific sublevels. Substructures of these parts of the spectra may arise as a consequence of the combined influence of quantum interference and the Freeman resonance. In each ATI order of the spectra, quantum interference and the Freeman resonance respectively dominate in the tail-like structure and the high-energy region of the main ATI peak, so it is reasonable to expect an intermediate region where both the two factors play nonignorable roles in the formation of the substructure.

We now turn to the effects of the pulse duration on the fine structures of the main ATI peaks, which are illustrated in Fig. 8. All spectra are produced by pulses of $I = 1.7 \times 10^{14} \text{ W/cm}^2$ and $\lambda = 400 \text{ nm}$. As expected, Freeman resonance peaks are insensitive to changes of the pulse duration. As the FWHM decreases from 0.4 ps through 0.2 ps to 0.1 ps (i.e., the number of cycles varies from about 300 through about 150 to about 75), a general tendency is that nearly all subpeaks become broader and less visible. Part of the subpeaks even disappear during the process. When the FWHM is decreased down to 0.1 ps, most of the still visible subpeaks are quite blunt. We have been aware of some of the spectra reported in Refs. [10,37], which were produced by pulses up to 20 fs. With those pulse lengths, the authors did not observe Freeman-resonance-induced sharp subpeaks, but only broadenings of the main ATI peaks. Considering both our numerical results and the previous studies, it is apparent that, to observe pronounced resonance-induced patterns in the electron spectrum, enough pulse length should be ensured. The reason is straightforward: a shorter pulse has a larger bandwidth, leading to broader resonance-induced subpeaks in the spectrum; given the narrow spacing between the subpeaks (because of the closely spaced Rydberg sublevels), they may merge with each other and cannot be distinguished. To our knowledge, full-dimensional TDSE calculations involving the Freeman resonance are not often seen for pulse lengths exceeding 0.1 ps. The present work hopefully could fit this gap. It is worthwhile to note that, in Ref. [59], the authors experimentally measured the electron spectra for ionization of a variety of small molecules. Distinct resonance peaks were seen even for pulses as short as 9 fs (less than four cycles). The surprising observation was attributed to the large variation in the multiphoton coupling strength between the ground state and different excited states. However, this phenomenon is beyond the scope of the present work.

D. Wavelength dependence

The results so far presented are limited to pulses of $\lambda = 400 \text{ nm}$. To study the wavelength dependence of substructures of the spectrum, we have performed calculations with $\lambda = 300, 608,$ and 800 nm at two different intensities $I = 1.2, 1.7 \times 10^{14} \text{ W/cm}^2$ while keeping FWHM = 0.4 ps unchanged, the results of which are shown in Fig. 9.

Figure 9(a) presents the first two ATI peaks of the spectra for $\lambda = 300 \text{ nm}$. At $1.7 \times 10^{14} \text{ W/cm}^2$, in contrast to the spectra for $\lambda = 400 \text{ nm}$, the peak splitting is almost absent.

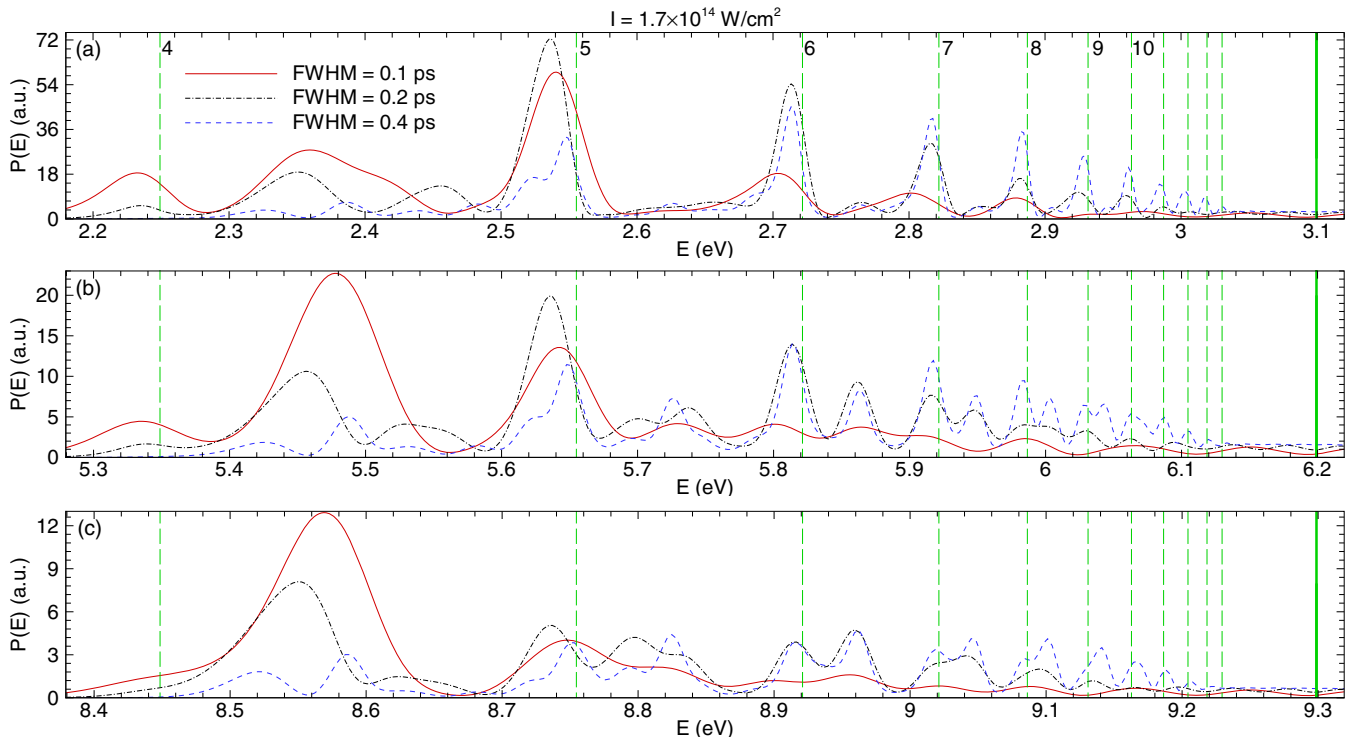


FIG. 8. Detailed structures of the first three main ATI peaks [plotted (in linear scale) in (a)–(c), respectively] in the spectra for pulses of identical peak intensities but varying durations. The vertical dashed lines mark subpeak positions predicted in the spirit of the Freeman resonance without considering the ac Stark shifts of the intermediate states. Integers next to the lines [shown in (a) only] are quantum numbers n of the intermediate states. The thicker vertical solid lines mark the predicted subpeak positions in the $n \rightarrow \infty$ limit.

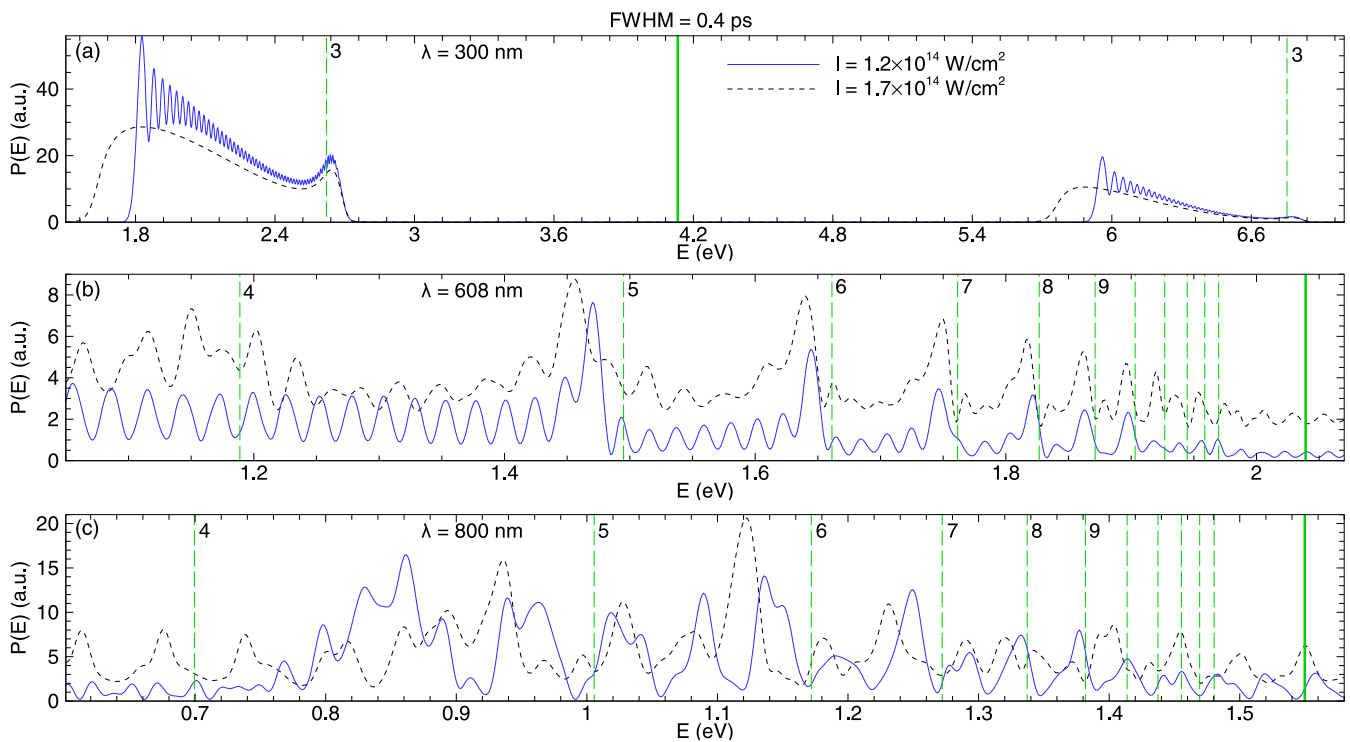


FIG. 9. Detailed structures (in linear scale) of the first two main ATI peaks for $\lambda = 300$ nm (a), the first main ATI peak for $\lambda = 608$ nm (b), and the first main ATI peak for $\lambda = 800$ nm (c) at two intensities. The vertical dashed lines mark subpeak positions predicted in the spirit of the Freeman resonance without considering the ac Stark shifts of the intermediate states. Integers next to the lines are quantum numbers n of the intermediate states. The thicker vertical solid lines mark the predicted subpeak positions in the $n \rightarrow \infty$ limit.

The first main ATI peak only has two subpeaks: the broader one is due to the direct ionization from the ground state, whereas the narrower one is identified as due to Freeman resonances of levels with $n = 3$, as denoted by the vertical dashed line. The resonance peak related to levels with $n = 3$ also appears in the second main ATI peak but is much more blurred. No interference-induced oscillations are identified in the spectrum at 1.7×10^{14} W/cm². At 1.2×10^{14} W/cm², the two subpeaks respectively attributable to the direct ionization and the Freeman resonance still exist in each of the first two main peaks. However, between the two subpeaks, interference-induced oscillations emerge. This is another manifestation that lower laser intensity enhances the interference. The reasons why the resonance-induced substructure is less prominent for shorter wavelength were already pointed out in Ref. [9] or [10]: due to the shorter wavelength (larger photon energy), fewer photons are absorbed in the ionization and therefore the chance of hitting a resonance decreases; moreover, as can be seen from Eq. (9), larger photon energy leads to smaller ponderomotive energy, thus fewer excited states are likely to shift into resonance.

Following the reasoning above, one would expect the resonance-induced substructure to be more pronounced for wavelengths exceeding 400 nm. However, the wavelength dependence is not that straightforward. In 1990, the Freeman resonance in atomic hydrogen was first experimentally studied by Rottke *et al.* [13], who in their paper presented an electron energy spectrum produced by a 608 nm 0.4 ps pulse with a peak intensity of $\sim 10^{14}$ W/cm². Several sharp subpeaks were observed and identified with Freeman resonances of atomic levels with $n \geq 4$. The main features of this spectrum were in the same year reproduced by Dörr *et al.* [36] through a Floquet theoretical calculation with $I = 1.2 \times 10^{14}$ W/cm². To make a comparison with the previous work, in Fig. 9(b), we plot the first ATI peaks of the spectra calculated for $\lambda = 608$ nm at two different intensities. The presented spectra are much more complicated than either the spectra reported in previous studies or our numerical results in the $\lambda = 400$ nm case. While several tall subpeaks can be clearly identified with Freeman resonances of intermediate levels (with $n \geq 5$), other subpeaks sandwiched between the Freeman resonance

subpeaks are attributed to quantum interference, for their high susceptibility to pulse intensity. In the experiment [13] and the Floquet theoretical calculation [36], the identified Freeman resonance peaks with the minimum n were those with $n = 4$. However, in Fig. 9(b), no subpeaks can be identified as related to levels with $n = 4$. Even after a careful search by performing calculations with intensities in the range of $0.3 - 5.0 \times 10^{14}$ W/cm², we still cannot reproduce the resonance peaks related to the $n = 4$ levels as presented in past experimental and theoretical studies. This disagreement between the present full-dimensional TDSE calculations and previous studies is left as an open question.

When the wavelength is increased up to 800 nm, the spectra even further complexify, as can be seen in Fig. 9(c). In this case, it is rather difficult to allocate subpeaks to particular intermediate sublevels, although some subpeaks seem to be resonance peaks because they do not change much in position when the intensity is varied. On the other hand, as discussed earlier, the interference substructure typically exhibits a regular oscillation, which does not occur in Fig. 9(c). The substructures resulting from the Freeman resonance are perhaps strongly entangled with those originating from quantum interference, leading to quite complicated electron energy spectra.

E. Pulse shape dependence

All results presented above are generated by using the sine-squared laser pulse. For its easy numerical implementation, this type of pulse is commonly used in the TDSE calculations, although the sine-squared envelope is quite artificial, deviating a lot from those conventionally used in strong-field experiments. Since only long pulses are involved in our calculations, it is expected that the pulse shape would not influence the results to a great extent. Nevertheless, we still wish to examine the dependence of the substructures of the electron spectrum on the pulse shape. To this end, we redo some of the calculations mentioned above using the Gaussian pulse, which can better approximate the temporal profiles of the laser field in real experiments. Then, we make a comparison between the spectra produced by pulses of the two different envelopes.

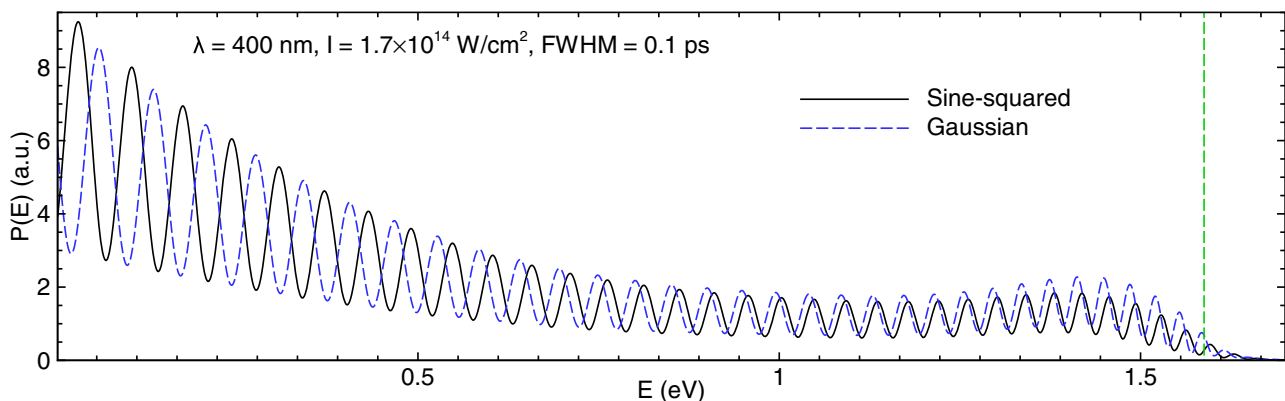


FIG. 10. Comparison of the detailed structures (in linear scale) of the first tail-like structures in the spectra generated by a sine-squared pulse and a Gaussian pulse with the same laser parameters. The vertical dashed line marks the energy position of the Freeman resonance peak related to levels with $n = 3$ predicted without considering the ac Stark shift.

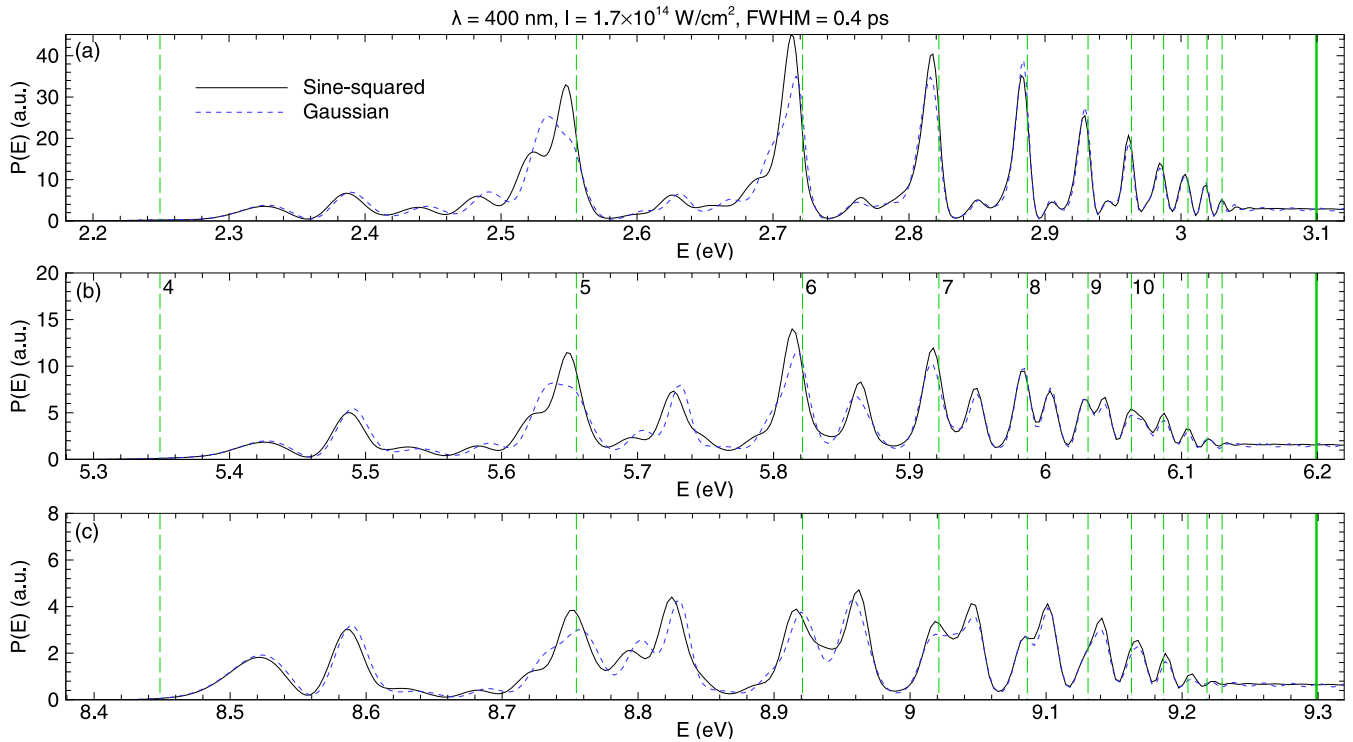


FIG. 11. Comparison of the detailed structures (in linear scale) of the first three main ATI peaks in the spectra generated by a sine-squared pulse and a Gaussian pulse with the same laser parameters. The vertical dashed lines mark subpeak positions predicted in the spirit of the Freeman resonance without considering the Stark shifts of the intermediate states. Integers next to the lines [shown in (b) only] are quantum numbers n of the intermediate states. The thicker vertical solid lines mark the predicted subpeak positions in the $n \rightarrow \infty$ limit.

At the same laser parameters, we can still obtain the type of energy spectrum shown in Fig. 2, in which the tail-like structures and the main ATI peaks are distributed alternately. The first tail-like structures (in expanded view) of the spectra generated by a sine-squared pulse and a Gaussian pulse with the same laser parameters ($\lambda = 400$ nm, $I = 1.7 \times 10^{14}$ W/cm², and FWHM = 0.1 ps) is compared in Fig. 10. Such laser parameters are chosen for the sake of good visibility of the interference substructures. Obviously, the two curves resemble each other in the overall shape, the amplitude of the oscillation, and the average spacing between subpeaks. However, the two curves exhibit subpeaks at different energy positions. This can be explained in the time-domain double-slit interference picture: obviously the phase difference between electron wave packets ejected at the two slits versus the ionized electron energy is modulated by the pulse shape.

As for the main ATI peaks, in Fig. 11, a comparison is made between the detailed structures of the first three main ATI peaks of the spectra produced by a sine-squared pulse and a Gaussian pulse with the same laser parameters ($\lambda = 400$ nm, $I = 1.7 \times 10^{14}$ W/cm², and FWHM = 0.4 ps). The laser parameters are chosen such that the Freeman-resonance-induced substructures are pronounced. As can be seen clearly, the two spectra exhibit strong resemblances to each other. Their overall shapes and signal strengths are both comparable. Especially, in the high-energy regions of the main ATI peaks, subpeaks of the two spectra almost occur at the same energy positions. In the low-energy regions, the two spectra show minor differences in subpeak positions.

Although the pulse shape has a modulation on electron spectrum, there are considerable resemblances between electron spectra produced by pulses of different shapes but the same laser parameters. The influences of the laser parameters (such as intensity, duration, and wavelength) on substructures of the spectrum should not be pulse shape dependent. As a result, our conclusions made for the sine-squared pulse can be straightforwardly extended to the Gaussian pulse.

IV. SUMMARY

In this article, by the full-dimensional TDSE calculations, we have studied the conjoint effects of quantum interference and the Freeman resonance on the fine structures of the spectra in ATI of atomic hydrogen by subpicosecond intense laser pulses. The recently proposed split-Lanczos propagator enables us to very efficiently deal with pulses much longer than those used in past full-dimensional TDSE calculations involving the Freeman resonance. Although our findings are mostly based on simulations using the sine-squared pulse, we have demonstrated that they are still valid in the case of the Gaussian pulse. Because of the universality of quantum interference and the Freeman resonance, similar results are expected in other systems, such as noble gas atoms.

We find that, at specific laser parameters, each ATI order of the electron energy spectrum is composed of two distinct parts—the tail-like structure and the main ATI peak. Both the two parts contain substructures. The low-lying and high-lying bound states play different roles in the formation of these

substructures. In the tail-like structure, the spectrum shows a fast oscillation, which we attribute to quantum interference between electron wave packets emitted from the low-lying bound states. The main ATI peak is observed to consist of many subpeaks, which are mostly the consequences of the Freeman resonance. By calculating the ac Stark energy shifts of the intermediate excited states, the energy positions of a number of subpeaks are perfectly explained in terms of the Freeman resonance.

The dominance of quantum interference and the Freeman resonance in different regions of the spectrum is heavily dependent on laser parameters such as the pulse intensity and wavelength. By adjusting the laser parameters, several special cases are found: (1) quantum interference and the Freeman resonance respectively dominate the low-energy and high-energy parts of the ATI orders; (2) both the two factors play little roles in the spectrum and the peak splitting is barely

seen; (3) only quantum interference plays noticeable roles in the spectrum; (4) both the two factors contribute to the high-energy parts of the ATI orders, giving rise to oscillatory interference substructures sandwiched between Freeman resonance subpeaks.

ACKNOWLEDGMENTS

This work is supported by the National Natural Science Foundation of China (NSFC) (Grants No. 11804233, No. 11575118, and No. 11747013), National Key Research and Development Project of China (Grant No. 2017YFF0106500), NSF of Guangdong (Grant No. 2018A0303130311), and Science and Technology plan project of Shenzhen (Grants No. KQJSCX20180328093801773, No. JCYJ20180305124540632, and No. JCYJ20190808121405740).

-
- [1] P. Agostini, F. Fabre, G. Mainfray, G. Petite, and N. K. Rahman, *Phys. Rev. Lett.* **42**, 1127 (1979).
- [2] P. Kruit, J. Kimman, and M. J. V. der Wiel, *J. Phys. B: At. Mol. Phys.* **14**, L597 (1981).
- [3] G. Petite, F. Fabre, P. Agostini, M. Crance, and M. Aymar, *Phys. Rev. A* **29**, 2677 (1984).
- [4] T. J. McIlrath, P. H. Bucksbaum, R. R. Freeman, and M. Bashkansky, *Phys. Rev. A* **35**, 4611 (1987).
- [5] M. Lein, J. P. Marangos, and P. L. Knight, *Phys. Rev. A* **66**, 051404(R) (2002).
- [6] A. D. Bandrauk, S. Chelkowski, and I. Kawata, *Phys. Rev. A* **67**, 013407 (2003).
- [7] N. Suárez, A. Chacón, M. F. Ciappina, B. Wolter, J. Biegert, and M. Lewenstein, *Phys. Rev. A* **94**, 043423 (2016).
- [8] N. Suárez, A. Chacón, E. Pisanty, L. Ortmann, A. S. Landsman, A. Picón, J. Biegert, M. Lewenstein, and M. F. Ciappina, *Phys. Rev. A* **97**, 033415 (2018).
- [9] V. C. Reed and K. Burnett, *Phys. Rev. A* **43**, 6217 (1991).
- [10] M. Wickenhauser, X. M. Tong, and C. D. Lin, *Phys. Rev. A* **73**, 011401(R) (2006).
- [11] R. R. Freeman, P. H. Bucksbaum, H. Milchberg, S. Darack, D. Schumacher, and M. E. Geusic, *Phys. Rev. Lett.* **59**, 1092 (1987).
- [12] P. Agostini, A. Antonetti, P. Breger, M. Crance, A. Migus, H. G. Muller, and G. Petite, *J. Phys. B: At. Mol. Opt. Phys.* **22**, 1971 (1989).
- [13] H. Rottke, B. Wolff, M. Brickwedde, D. Feldmann, and K. H. Welge, *Phys. Rev. Lett.* **64**, 404 (1990).
- [14] H. Rottke, B. Wolff-Rottke, D. Feldmann, K. H. Welge, M. Dörr, R. M. Potvliege, and R. Shakeshaft, *Phys. Rev. A* **49**, 4837 (1994).
- [15] G. D. Gillen and L. D. Van Woerkom, *Phys. Rev. A* **68**, 033401 (2003).
- [16] E. Mevel, P. Breger, R. Trainham, G. Petite, P. Agostini, J. P. Chambaret, A. Migus, and A. Antonetti, *J. Phys. B: At. Mol. Opt. Phys.* **25**, L401 (1992).
- [17] M. Nakano, T. Otake, and R. Itakura, *Phys. Rev. A* **95**, 063404 (2017).
- [18] P. V. Demekhin and L. S. Cederbaum, *Phys. Rev. Lett.* **108**, 253001 (2012).
- [19] P. V. Demekhin and L. S. Cederbaum, *Phys. Rev. A* **88**, 043414 (2013).
- [20] M. Bagheri, U. Saalmann, and J. M. Rost, *Phys. Rev. Lett.* **118**, 143202 (2017).
- [21] W.-C. Jiang, S.-G. Chen, L.-Y. Peng, and J. Burgdörfer, *Phys. Rev. Lett.* **124**, 043203 (2020).
- [22] W.-C. Jiang and J. Burgdörfer, *Opt. Express* **26**, 19921 (2018).
- [23] M.-X. Wang, H. Liang, X.-R. Xiao, S.-G. Chen, W.-C. Jiang, and L.-Y. Peng, *Phys. Rev. A* **98**, 023412 (2018).
- [24] R. R. Freeman and P. H. Bucksbaum, *J. Phys. B: At. Mol. Opt. Phys.* **24**, 325 (1991).
- [25] A. Rudenko, K. Zrost, C. D. Schröter, V. L. B. de Jesus, B. Feuerstein, R. Moshhammer, and J. Ullrich, *J. Phys. B: At. Mol. Opt. Phys.* **37**, L407 (2004).
- [26] M. Fushitani, C.-N. Liu, A. Matsuda, T. Endo, Y. Toida, M. Nagasono, T. Togashi, M. Yabashi, T. Ishikawa, Y. Hikosaka, T. Morishita, and A. Hishikawa, *Nat. Photon.* **10**, 102 (2016).
- [27] P. Ludowise, M. Blackwell, and Y. Chen, *Chem. Phys. Lett.* **258**, 530 (1996).
- [28] W. Guo, Y. Wang, and Y. Li, *Optik* **161**, 151 (2018).
- [29] N. P. Moore and R. J. Levis, *J. Chem. Phys.* **112**, 1316 (2000).
- [30] M. Goto and K. Hansen, *Chem. Phys. Lett.* **522**, 23 (2012).
- [31] X. Tang, A. Lyras, and P. Lambropoulos, *Phys. Rev. Lett.* **63**, 972 (1989).
- [32] Y. Gontier and M. Trahin, *Phys. Rev. A* **46**, 1488 (1992).
- [33] D. S. Guo, Y. S. Wu, and L. Van Woerkom, *Phys. Rev. A* **73**, 023419 (2006).
- [34] Y. Wang, J. Zhang, Z. Xu, Y.-S. Wu, J. T. Wang, and D.-S. Guo, *Phys. Rev. A* **80**, 053417 (2009).
- [35] M. Dörr and R. Shakeshaft, *Phys. Rev. A* **38**, 543 (1988).
- [36] M. Dörr, R. M. Potvliege, and R. Shakeshaft, *Phys. Rev. A* **41**, 558 (1990).
- [37] Q. Li, X.-M. Tong, T. Morishita, H. Wei, and C. D. Lin, *Phys. Rev. A* **89**, 023421 (2014).
- [38] X. Gong, C. Lin, F. He, Q. Song, K. Lin, Q. Ji, W. Zhang, J. Ma, P. Lu, Y. Liu, H. Zeng, W. Yang, and J. Wu, *Phys. Rev. Lett.* **118**, 143203 (2017).
- [39] R. Wiehle, B. Witzel, H. Helm, and E. Cormier, *Phys. Rev. A* **67**, 063405 (2003).
- [40] T. Morishita and C. D. Lin, *Phys. Rev. A* **87**, 063405 (2013).

- [41] P. Hansch, M. A. Walker, and L. D. Van Woerkom, *Phys. Rev. A* **55**, R2535 (1997).
- [42] M. P. Hertlein, P. H. Bucksbaum, and H. G. Muller, *J. Phys. B: At. Mol. Opt. Phys.* **30**, L197 (1997).
- [43] H. G. Muller, *Phys. Rev. A* **60**, 1341 (1999).
- [44] H. G. Muller, *Phys. Rev. Lett.* **83**, 3158 (1999).
- [45] J. Wassaf, V. Vénier, R. Taïeb, and A. Maquet, *Phys. Rev. Lett.* **90**, 013003 (2003).
- [46] R. M. Potvliege and S. Vučić, *J. Phys. B: At. Mol. Opt. Phys.* **42**, 055603 (2009).
- [47] L. Xu and L. Fu, *Phys. Rev. Lett.* **122**, 253202 (2019).
- [48] R. A. Blank and M. Shapiro, *Phys. Rev. A* **51**, 4762 (1995).
- [49] W.-C. Jiang and X.-Q. Tian, *Opt. Express* **25**, 26832 (2017).
- [50] T. N. Rescigno and C. W. McCurdy, *Phys. Rev. A* **62**, 032706 (2000).
- [51] M. J. Rayson, *Phys. Rev. E* **76**, 026704 (2007).
- [52] B. I. Schneider and L. A. Collins, *J. Non-Cryst. Solids* **351**, 1551 (2005).
- [53] X. M. Tong, K. Hino, and N. Toshima, *Phys. Rev. A* **74**, 031405(R) (2006).
- [54] A. Scrinzi, *New J. Phys.* **14**, 085008 (2012).
- [55] L. Tao and A. Scrinzi, *New J. Phys.* **14**, 013021 (2012).
- [56] A. Zielinski, V. P. Majety, and A. Scrinzi, *Phys. Rev. A* **93**, 023406 (2016).
- [57] C. J. Joachain, N. J. Kylstra, and R. M. Potvliege, *Atoms in Intense Laser Fields* (Cambridge University Press, Cambridge, UK, 2012).
- [58] N. B. Delone and V. P. Krainov, *Phys. Usp.* **42**, 669 (1999).
- [59] V. Tagliamonti, P. Sándor, A. Zhao, T. Rozgonyi, P. Marquetand, and T. Weinacht, *Phys. Rev. A* **93**, 051401(R) (2016).